

RESEARCH ARTICLE

Amniotic fluid stem cell-derived extracellular vesicles are independent metabolic units capable of modulating inflammasome activation in THP-1 cells

Letizia Mezzasoma¹  | Ilaria Bellezza¹  | Pierluigi Orvietani¹ | Giorgia Manni¹  | Marco Gargaro¹  | Krizia Sagini²  | Alicia Llorente²  | Paolo Scarpelli¹  | Luisa Pascucci³  | Barbara Cellini¹  | Vincenzo Nicola Talesa¹ | Francesca Fallarino¹  | Rita Romani¹ 

¹Department of Medicine and Surgery, University of Perugia, Polo Unico Sant'Andrea delle Fratte, Perugia, Italy

²Department of Molecular Cell Biology, Institute for Cancer Research, Oslo University Hospital, The Norwegian Radium Hospital, Oslo, Norway

³Department of Veterinary Medicine, Perugia, Italy

Correspondence

Rita Romani, Department of Medicine and Surgery, University of Perugia, Polo Unico Sant'Andrea delle Fratte, P.e Lucio Severi 1, Perugia 06132, Italy.
Email: rita.romani@unipg.it

Funding information

Department of Medicine and Surgery, Perugia University

Abstract

An immunoregulatory role of stem cells, often mediated by their secretome, has been claimed by several studies. Stem cell-derived extracellular vesicles (EVs) are crucial components of the secretome. EVs, a heterogeneous group of membranous vesicles released by many cell types into the extracellular space, are now considered as an additional mechanism for intercellular communication. In this study, we aimed at investigating whether human amniotic stem cell-derived extracellular vesicles (HASC-EVs) were able to interfere with inflammasome activation in the THP-1 cell line. Two subsets of HASC-EVs were collected by sequential centrifugation, namely HASC-P10 and HASC-P100. We demonstrated that HASC-EVs were neither internalized into nor undertake a direct interaction with THP-1 cells. We showed that HASC-P10 and P100 were able to intrinsically produce ATP, which was further converted to adenosine by 5'-nucleotidase (CD73) and ectonucleoside triphosphate diphosphohydrolase-1 (CD39). We found that THP-1 cells conditioned with both types of HASC-EVs failed to activate the NLRP3/caspase-1/inflammasome platform in response to LPS and ATP treatment by a mechanism involving A2a adenosine receptor activation. These results support a role for HASC-EVs as independent metabolic units capable of modifying the cellular functions, leading to anti-inflammatory effects in monocytic cells.

Abbreviations: ADO, adenosine; ADP, adenosine 5'-triphosphate disodium salt; AK, adenylate kinase; AMP, adenosine 2'-monophosphate; ATP, adenosine 5'-triphosphate disodium salt hydrate; CD39, ectonucleoside triphosphate diphosphohydrolase-1; CD73, ATPase, 5'-nucleotidase; CGS-21680, 4-[2-[[[6-Amino-9-(N-ethyl-β-D-ribofuranuronamidoyl)-9H-purin-2-yl]amino]ethyl]benzenepropanoic acid; HASC, human amniotic fluid stem cells; LPS, lipopolysaccharide; NECA, N-ethylcarboxamidoadenosine; NLRP3, NOD-like receptor protein 3; ZM241385, 4-(2-[7-Amino-2-(2-furyl)[1,2,4]triazolo[2,3-a][1,3,5]triazin-5-ylamino]ethyl)phenol.

Letizia Mezzasoma and Ilaria Bellezza contributed equally to this work.

This is an open access article under the terms of the Creative Commons Attribution License, which permits use, distribution and reproduction in any medium, provided the original work is properly cited.

© 2022 The Authors. *The FASEB Journal* published by Wiley Periodicals LLC on behalf of Federation of American Societies for Experimental Biology

KEYWORDS

ATP production, immunoregulation, inflammasomes, stem cell-derived extracellular vesicles

1 | INTRODUCTION

Extracellular vesicles (EVs) are a heterogeneous family of lipid bilayer-vesicular structures that are released by nearly all living cells and can perform a wide range of critical biological functions.¹ As carriers of biologically active molecules including proteins, lipids, and nucleic acids, EVs mediate cell-to-cell communication and execute diverse functions by delivering their cargoes to specific cell types in both normal and pathological conditions, including cancer, angiogenesis, cellular differentiation, osteogenesis, and inflammation.^{2–6} EVs transmit information and activate biological responses in target cells through several potential mechanisms: (i) direct fusion with the plasma membrane and release of the exosomal content; (ii) uptake of intact exosomes into endosomes and subsequent release of the content into the cytoplasm; (iii) juxtacrine signaling between ligands expressed on exosomes and cognate receptors on target cells, without intracellular delivery of cargo.^{7,8}

A growing body of evidence supports a key role for EVs in regulating metabolic homeostasis or associated cellular processes.⁹ A pivotal role attributed to EVs is the propagation of specific metabolic signals to the surrounding cells in the microenvironment. For instance, glucose deprivation has been shown to promote the trafficking of glucose transporters and glycolytic enzymes between cardiomyocytes through EVs.¹⁰ Iraci et al. demonstrated that neural stem/progenitor cell (NSC)-derived EVs exhibit L-asparaginase activity.⁹ Prostate-derived EVs harbor enzymes involved in adenosine triphosphate (ATP) metabolic turnover which is involved in EVs uptake by prostate cancer cells.¹¹ Although it has been shown that cells can traffic metabolic enzymes via EVs, much remains to be clarified regarding the impact of their metabolic activity.

Several studies have highlighted an immunoregulatory role for stem cells (SCs) and their secreted EVs.^{4,12,13} Although the remarkable ability of SCs to promote tissue repair and regeneration has long been attributed to their proficiency to differentiate into other cell types upon environmental cues, it has become clear that SCs can exert most of their reparative, angiogenic and immunosuppressive functions through paracrine mediators, involving soluble factors and EVs.¹⁴ Therefore, SC-derived EVs are now of great interest as an alternative to stem cells in specific MSC-based therapeutic approaches and have shown promising effects in various autoimmune disorders.^{12,15,16}

Maturation of IL-1 β by caspase-1 mediated cleavage is a key inflammatory event. Caspase-1 itself is synthesized as an inactive 45 kDa zymogen (pro-caspase-1) that undergoes autocatalytic processing following an appropriate stimulus.¹⁷ Caspase-1 is activated within multiprotein complexes, named inflammasomes. Inflammasomes recognize various inflammation-inducing stimuli, such as endogenous danger/damage-associated molecular patterns (DAMPs) and exogenous pathogen-associated molecular patterns (PAMPs). They tightly regulate the production of proinflammatory cytokines, such as IL-1 β and IL-18¹⁸ by activating caspase-1 through interaction with ASC (apoptosis-associated speck-like protein containing a carboxy-terminal CARD), an adapter protein that bridges NOD-like receptor (NLRs) and caspase-1.¹⁹ Canonical NOD-like receptor protein 3 (NLRP3) is the most studied and best-known inflammasome receptor, which senses multiple microbial and endogenous danger signals.²⁰ Inflammasomes are now recognized as key mediators of acute and chronic inflammatory responses involving macrophages and dendritic cells. Moreover, a recent study demonstrated that EVs can be involved in inflammasome activation in cells of prostatic origin.²¹

The objective of this study was to investigate whether EVs derived from human amniotic fluid stem cells (HASC-EVs) have an intrinsic metabolic activity that could exert functional roles either directly or indirectly, through the autonomous production of active biomolecules. We have demonstrated for the first time that HASC-EVs possess intrinsic metabolic activities and that the generated metabolic products influence the phenotype of the human monocytic cell line THP-1 through the production of adenosine.

2 | MATERIALS AND METHODS

2.1 | Reagents

All the chemicals used in the present study were analytical grade reagents from various sources. LPS (Lipopolysaccharide from *Escherichia coli* 0111:B4), ATP (Adenosine 5'-triphosphate disodium salt hydrate), ADP (Adenosine 5'-triphosphate disodium salt), AMP (Adenosine 2'-monophosphate), ADO (Adenosine), glutaraldehyde solution, osmium tetroxide were purchased from Sigma-Aldrich (Milan, Italy).

Acetonitrile (HPLC grade) was from J.T.Baker, ammonium acetate was from Carlo Erba Analyticals. All reagents used for the HPLC were dissolved in ultra-pure water and then filtered with a 0.45- μm Durapore Membrane Filters (Millipore).

The non-specific adenosine receptor agonist N-ethylcarboxamidoadenosine (NECA), the selective adenosine A2a receptor agonist CGS-21680 (4-[2-[[6-Amino-9-(N-ethyl- β -D-ribofuranuronamidoyl)-9H-purin-2-yl]amino]ethyl]benzenepropanoic acid) and the selective A2A receptor antagonist ZM241385 (4-(2-[7-Amino-2-(2-furyl)[1,2,4]triazolo[2,3-a][1,3,5]triazin-5-ylamino]ethyl)phenol) were obtained from Tocris Bioscience (Bristol, UK) and dissolved in dimethyl sulfoxide (DMSO). BS(PEG)5 (PEGylated bis(sulfosuccinimidyl)suberate) and DiL (1,1'-Dioctadecyl-3,3',3'-Tetra methylindocarbocyanine Perchlorate) were from Thermo Fisher Scientific (Waltham, MA, USA). Unless otherwise stated, all the antibodies were from Cell Signaling Technology (Danvers, MA, USA), and all cell culture reagents were from Invitrogen (Milan, Italy).

2.2 | HASCs isolation and culture

HASCs were obtained from human amniotic fluids of 16–17-week pregnant women (aged 35–40 years), who underwent amniocentesis during routine prenatal diagnosis. The study was approved by the University of Perugia Bioethics Committee, and each participant provided informed consent for the secondary use of amniotic fluid samples. The isolation was performed according to Romani et al.¹²

2.3 | Isolation of HASC-derived EVs

EVs isolation was performed according to Romani et al.¹² Briefly, serum-free conditioned medium (MSCBM Lonza, Milan Italy # PT-3238 with L-glutamine and gentamicin sulfate/amphotericin B) from 5×10^6 HASCs (passage 4–5) after 24 h culture, was pooled and centrifuged at 300 g for 10 min, then at 2000 g for 20 min, followed by centrifugation at 10 000 g for 45 min, the pellet was saved as HASC-P10 fraction and the supernatant was ultracentrifuged at 100 000 g for 60 min in an Optima TLX ultracentrifuge with a 60Ti rotor (Beckman Coulter, USA) and the pellet saved as HASC-P100. HASC-P10 and HASC-P100 pellets were washed by ultracentrifugation at 100 000 g for 60 min with PBS containing 1% penicillin/streptomycin. We used sterile certified centrifuge tubes free of any detectable DNA, DNase, RNase, PCR inhibitors, and endotoxins (Beckman Coulter, USA) and sterile practices. The

pellets were suspended at 1 mg/ml concentration with endotoxin-free PBS (Merck, Darmstadt, Germany) added with 1% penicillin/ and streptomycin to avoid potential microbial contamination and stored at -80°C until further use. All samples were tested for their endotoxin level with Pierce™ LAL Chromogenic Endotoxin Quantitation Kit (Thermo Scientific, San Jose, CA, USA). All the samples used in the study have endotoxin levels below the detection limit.

2.4 | Nanoparticle tracking analysis (NTA)

HASC-P10 and HASC-P100 pellets were resuspended in PBS (filtered through a 0.02 μm Anotop 25 filter) to obtain a concentration within the recommended range (2×10^8 – 1×10^9 particles per ml). Samples were vortexed for 1 min and then loaded into a NS500 instrument (Malvern Instruments Ltd, Worcestershire, UK). For each sample, 5 videos of 60 sec were acquired and processed using the NTA2.3 software. Particles moving under Brownian motion were tracked and their hydrodynamic diameter was calculated using the Stokes-Einstein equation.

2.5 | Scanning Electron Microscopy (SEM) analysis

EVs were fixed in 1.5% glutaraldehyde for 15 min at room temperature, washed with water, sedimented on glass coverslips, and then allowed to dry at room temperature. SEM images were obtained using a field emission gun electron scanning microscope (LEO 1525 Zeiss; Thomwood NY, USA) with Cr metallization using a high-resolution sputter 150T ES-Quorum apparatus (24 s, sputter at a current of 240 mA). Chromium thickness was ~ 10 nm.

2.6 | Transmission Electron Microscope (TEM) analysis

HASCs were detached from the flask by trypsin-EDTA and fixed with 2.5% glutaraldehyde in 0.1 M phosphate buffer (PB; sodium chloride, 150 mM, and sodium phosphate, 150 mM pH 7.3), for 1 h at 4°C . Cells were washed in PB and centrifuged at 300 g for 10 min to remove the fixative. After washing twice with PB, the pellet was post-fixed in 2% osmium tetroxide, dehydrated in a graded series of ethanol up to absolute, and embedded in Epon 812. Ultrathin sections (90 nm) were mounted on 200-mesh copper grids, stained with uranyl acetate and lead citrate, and examined

under a Philips EM 208 transmission electron microscope (TEM) equipped with a digital camera (University Centre for Electron Microscopy [CUME]—Perugia).

2.7 | Proteomics analysis

HASC-P10 and HASC-P100 were separated on 6%–15% polyacrylamide gels and then stained with Oriole Fluorescent gel stain (Bio-Rad, Hercules, California USA). The whole gel was sliced in 21 bands (approximately 3×5 mm) for each lane using a Versadoc 1000 instrument (Bio-Rad, Hercules, CA, USA). The bands were washed and gradually dehydrated twice in 100 mM ammonium bicarbonate (ABC)/50% acetonitrile (ACN), in 50 mM ABC/50% ACN and in 25 mM ABC/50% ACN.

Cysteine bonds were reduced by incubation with 10 mM DTT/25 mM ABC at 56°C for 1 h and alkylated with 50 mM iodoacetamide/25 mM ABC at room temperature for 45 min in the dark, washed in water, and dried in a vacuum centrifuge. Gel cubes were incubated overnight with 6.25 ng/ml trypsin in ABC at 37°C to allow digestion. The supernatants were recovered, and peptides were extracted twice in 0.1% formic acid/60% ACN and dried in a vacuum centrifuge. Peptides were then resuspended in 100 μ l of loading buffer (5% ACN/0.1% formic acid).

Oligopeptides were separated using a ProteomeX apparatus (Thermo Scientific, San Jose, CA, USA) equipped with a 100 μ l loop and a Hypersil-Keystone BioBasic C18 capillary column (0.18 \times 100 mm) and configured in the Protein ID mode. The oligopeptide mixtures were injected in the RP-column equilibrated with 0.1% formic acid (solvent A) and separated with a gradient of ACN containing 0.1% formic acid (solvent B), at a flow rate of 2 μ l/min. After column injection, oligopeptides were eluted with a 35 min linear gradient from 5 to 60% solvent B, followed by a 5 min linear gradient from 60 to 80% solvent B and 8 min isocratic elution with 80% solvent B. Columns were equilibrated 20 min with solvent A before loading next sample. Eluted oligopeptides were electrosprayed directly into the LCQ Deca-XP^{Plus} ion-trap mass spectrometer. Database searching was performed by the MASCOT software version 2.2 (<http://www.matrixscience.com/>).²² Bioinformatic analysis of the proteomics data was performed by means of FUNRICH software.²³

2.8 | THP-1 cell culture and drug treatments

Human THP-1 monocytes were purchased from American Type Culture Collection (ATCC, USA) and routinely maintained at 37°C in 5% CO₂ in RPMI 1640 supplemented

with 10% heat-inactivated FBS, L-glutamine, 1 mM sodium pyruvate, non-essential amino acids, 1% of penicillin/streptomycin. THP-1 cells (3×10^6 cells/well) were plated in 12-well culture dishes, pretreated for 1 h with 100 μ g/ml HASC-derived EV-P10 (HASC-P10) or EV-P100 (HASC-P100), corresponding to approx. 1×10^2 and 2×10^2 EVs/cell, respectively. THP-1 cells were subsequently primed with 10 μ g/ml LPS for 20 min and then activated with 5 mM ATP for 40 min. The concentration of EVs has been chosen on the basis of previous experiences.^{21,24} In independent experiments, THP-1 cells were treated with 1 μ M NECA or with 100 μ M CGS-21680 for 2 h, or with 500 nM ZM241385 1 h before treatments. Vehicle-treated cells (DMSO) did not show any significant difference with respect to untreated control cells; therefore, all the relative treatments were compared to these latter controls.

At the end of the treatments, total cell lysates were prepared using RIPA buffer with protease and phosphatase inhibitors.

2.9 | Western blot analysis

Total THP-1 cell lysates (10 μ g) were separated by 8% or 12% sodium dodecyl sulfate-polyacrylamide gel electrophoresis (SDS-PAGE) and transferred on nitrocellulose membrane. Non-specific binding sites were blocked in Roti-Block (Roth GmbH) for 1 h at room temperature. The membranes were blotted overnight at 4°C with the following anti-human Abs diluted in Roti-Block: anti-ALIX(1A12; sc-53540) mouse monoclonal antibody (mAb) (Santa Cruz Biotechnology); anti-TGS101(C-2; sc-7964) mAb (Santa Cruz Biotechnology); anti-CD81 (B-11;sc-166029) mAb (Santa Cruz Biotechnology); anti-ARF6 (3A-1; sc7971) mAb (Santa Cruz Biotechnology); anti-Lamin A/C (346; sc-7293) mAb (Santa Cruz Biotechnology); anti-COX IV (F-8; sc-376731) mAb (Santa Cruz Biotechnology); anti-GAPDH (D16H11) mAb; anti-pyruvate kinase mAb (#4053); anti-NLRP3 (D4D8T) mAb (#15101); anti-Caspase-1 polyclonal antibody (pAb) (#2225); anti-IL-1 β (3A6) pAb (#12242); anti-ASC/TMS1 (E1E31) (#13833) mAb; anti-AIM2 (D5X7K) (#15101) mAb; anti-A2aR (7F6-G5-A2) mAb (#32261) (Cell Signalling Technology); anti-phospho-NLRP3 (Ser295) pAb (#5071SL) (Thermo Fisher Scientific, USA). After washing with TBST, blots were incubated for 1 h at room temperature with the appropriated HRP-conjugated secondary Abs and revealed using the enhanced chemi-luminescence (ECL) system (Amersham Pharmacia Biotech). Membranes were stripped and re-probed with anti- β -actin mAb (I-19) antibody (Santa Cruz Biotechnology) as the loading control. Densitometric analyses were performed with ImageJ software.

ASC crosslinking was performed with BS(PEG)5 according to the manufacturer's guidelines. Briefly, cells were resuspended in PBS (pH 7.2), frozen, thawed 5 times, and centrifuged for 10 min at 10 000 g at 4°C. Pellets were gently resuspended in 50 μ l of PBS (pH 7.2). Subsequently, 1 μ l of a BS(PEG)5 250 mM to a final concentration of 5 mM was added and incubated for 30 min at room temperature. In the end, 5 μ l TRIS 500 mM (pH 7.5) was added, incubated for 15 min at room temperature, and centrifuged for 10 min at 10 000 g at 4°C. Pellets were resuspended in 20 μ l loading buffer and resolved on a 12% SDS-PAGE and visualized by immunoblotting with an anti-ASC antibody.

2.10 | ATP measurement

ATP measurement was performed with an *in vitro* assay, 20 μ g EVs and HASC cells (positive controls) were incubated in "glycolytic buffer" containing: 10 mM $MgCl_2$, 10 mM KCl, 10 mM β -nicotinamide adenine dinucleotide (NAD^+), 10 mM DTT, 50 μ M ADP in PBS. The mixture was preincubated for 10 min at 37°C. Preincubated EVs were separately incubated with selected effectors (5 mM glucose, 20 mM 2-deoxyglucose, 10 mM sodium tartrate, 1 mM sodium fluoride, 1 mM rameic sulfate) for 30 min at 37°C to examine ATP formation under various conditions. Then, 10 μ l of the mixture were used to determine ATP concentration by an ATP determination kit (Molecular Probes, Eugene, OR, USA) following the manufacturer's instruction. In independent experiments, ADP or NAD^+ were omitted from the glycolytic buffer or EVs were pre-treated for 1 h with 50 μ g/ml proteinase K that was subsequently blocked with 2 mM PMSF.

2.11 | Lactate determination

Twenty micrograms HASC-P10 and P100 were incubated in the glycolytic buffer for 30 min, then treated with TCA (10% v/v) and centrifuged at 12 000 g for 3 min. Supernatants were incubated with LDH reaction buffer (280 mM hydrazine, 467 mM glycine, 2.6 mM ethylenediaminetetraacetic acid, 2.5 mM NAD^+ , 500 units L-lactic dehydrogenase used), and spectrophotometrically monitored at 340 nm. Results were expressed as mM of lactate was released. A lactate standard curve was prepared for each determination.

2.12 | FACS analyses

To determine the expression of CD39 and CD73 HASC-P10 and HASC-P100 staining with CD39-PE—or CD73-FITC

conjugated antibodies was performed according to standard protocols; the samples were washed in PBS and centrifuged for 1 h at 100 000 g to recover EVs. The two EVs subsets were analyzed on an EPICS flow cytometer using the EXPO 32 ADC software (Beckman Coulter, Pasadena, CA, USA).

For the detection of EVs uptake, HASC-P10 and HASC-P100 were stained for 30 min with 50- μ M DiL, washed by ultracentrifugation at 100 000 g for 1 h. The pellet was resuspended at 1 mg/ml in PBS supplemented with 1% penicillin/streptomycin solution. THP-1 cells (3×10^5) were exposed to labeled EVs for 2 h and DiL-labeled positive cells were determined by FACS. Samples were run on LSRFortessa (BD Biosciences, Franklin Lakes, NJ, USA) flow cytometer and analyzed using FlowJo analysis software.

Crosslinking was performed with BS(PEG)5, according to the manufacturer's guidelines. Briefly, THP-1 cells (3×10^5) were exposed to HASC-P10 and HASC-P100 in 500 μ l of the medium, 10 μ l of 250 mM BS(PEG)5 was added and incubated for 30 min at room temperature. After centrifugation at 10 000 g at 4°C for 10 min, pellets were resuspended in 500 μ l of buffer for flow cytometry analysis (PBS with 1% paraformaldehyde and 4% FBS).

2.13 | Florescence microscopy analyses

THP-1 cells, seeded on glass coverslips, were exposed to 100 μ g/ml of DiL-stained -EVs. After 2 h, cells were fixed with 4% PFA for 20 min at room temperature, and the membrane was stained with CellMask™ Green Plasma Membrane (Thermofisher scientific, USA) for 30 min at room temperature. Cell nuclei were counterstained with 4',6'-diamidino-2phenylindole (DAPI). Cells were then rinsed in PBS, mounted, and analyzed with a Zeiss Axio Observer Z1 equipped with Apotome and digital Camera Axiocam MRm (Zeiss, Oberkochen, Germany).

2.14 | Adenosine detection by HPLC analyses

20 μ l of ATP, ADP, AMP, and ADO standards (55 μ g/ml) were used for HPLC analysis. Mobile phase A consisted of 7 mM ammonium acetate buffer, adjusted to pH 3.0 with hydrochloric acid, while mobile phase B consisted of 100% acetonitrile. The HPLC analysis was carried out on an integrated JASCO LC-4000 system (ASCO Corporation, Ishikawamachi Hachioji-shi Tokyo Japan), which consisted of a quaternary pump equipped with an on-line vacuum degasser, and an UV/VIS detector. Chromatographic separations were performed on a NUCLEOSIL 100–5 C18

column (5 μm , 250 \times 4.6 mm) (Agilent technology, Santa Clara, CA, USA), at 22°C. HPLC separation was achieved using a continuous gradient elution. The elution program (25 min total) was as follows: 0 min 97% A, 3%B; 3–15 min 90%A, 10%B; 15–16 min 2%A, 98%B; 16–19 min 2%A, 98%B; 19–20 min 98%A, 2%B; 20–25 min 97%A, 3%B. The flow rate of the mobile phase was 1 ml/min, UV detection was set to 260 nm, while the injection volume was 20 μl .

2.15 | Statistical analysis

All analyses were performed using Prism version 6.0 (GraphPad Software). Results are expressed as means \pm SD from at least three independent experiments and were evaluated by Student's *t*-test or non-parametric test (one-way-ANOVA with Dunnett's Multiple Comparison test). A *p* value less than .05 was considered significant.

3 | RESULTS

3.1 | Characterization of HASC-EVs

Recent stem cell research suggests that EVs released by stem cells reflect the same regenerative potential and immunomodulatory capacity as their parental cells.²⁵ We used previously characterized human amniotic stem cells (HASC)¹² as a cell source to isolate EVs. TEM analyses of HASCs showed the presence of exosome-containing multivesicular bodies in the cytoplasm (Figure 1A,B) and ectosome release from the plasma membrane (Figure 1C) indicating that HASCs produce both ectosomes and exosomes. In this study, we named both vesicle types as EVs. HASC-EVs were isolated from serum-free cell culture media by differential centrifugation, following the protocol depicted in Figure 1D, and then subjected to specific characterization. Two fractions indicated as HASC-P10 (sedimented at 10 000 g) and HASC-P100 (sedimented at 100 000 g) were recovered. SEM analysis revealed the presence of EVs with a mean diameter of 60 \pm 10 nm for HASC-P10 and 60 \pm 20 nm for HASC-P100 (Figure 1E–H), whereas NTA analysis indicated a mean diameter of 163 \pm 16.53 nm for HASC-P10 and 156 \pm 18.60 nm for HASC-P100 (Figure 1I). Differences in sample preparation, and in particular the dehydration steps required for SEM analysis, may explain the discrepancies observed between the results of the two analysis methods. Nevertheless, both methods did not detect any significant dimensional differences between the two fractions. The profile of HASC-P10 and HASC-P100 size distribution are similar (Figure 1J). Both analyses showed that the two fractions were homogeneous in dimension and, according to O'Connell

et al.,²⁶ Takov et al.,²⁷ Balbi et al.,²⁸ no large vesicles (range >250 nm) were detected. Moreover, the number of particles/mg was higher in the HASC-P100 fraction as compared to the HASC-P10 fraction (Figure 1K). The number of particles/producing cell was $2.3 \times 10^2 \pm 0.85 \times 10^2$ particles/cell and $3.5 \times 10^2 \pm 0.74 \times 10^2$ particles/cell in HASC-P10 and HASC-P100, respectively, in agreement with reports in the literature.²⁷ Biochemical characterization of EVs confirmed the expression of EV marker proteins, including Alix (ALG-2 interacting protein X), CD81 (Tetraspanin-28), and TSG101 (Tumor susceptibility gene 101) (Figure 1K). HASC-P10 and HASC-P100 preparation did not contain markers characteristic of cellular organelles, such as lamin A/C, for the nucleus and COX IV for the mitochondria (Figure 1L), indicating that intracellular organelles were not co-isolated with EVs.

To further characterize the HASC-EVs, we conducted a qualitative proteomic analysis. The complete list of proteins detected in HASC-EVs is shown in Table S1. 95 proteins were detected in HASC-P10 and 59 were identified in HASC-P100, with 42 proteins in common between the two EVs subsets (Figure 2A).

FUNRICH software comparison with the 100 proteins most frequently described in EVs (source Vesiclepedia: <http://microvesicles.org/>) revealed 36 out of 95 and 27 out of 59 common proteins in HASC-P10 and HASC-P100 fraction, respectively (Figure 2B). The main biological processes in which EVs proteins are involved include signal transduction pathways and cell growth (Figure 2C). Furthermore, proteins involved in metabolism or protein associated with immune responses were also identified (Figure 2C). Notably, proteomic analysis, revealed that both HASC-P10 and HASC-P100 contained the enzymes of the glycolysis pay-off phase (Figure 2B), such as glyceraldehyde 3-phosphate dehydrogenase (GAPDH) and pyruvate kinase whose presence was further validated by western blot analysis (Figure 2D). β -actin and ARF6, identified by proteomic analysis, were also validated by western blotting analyses (Figure 2D).

3.2 | HASC-EVs produce ATP and adenosine

It has been demonstrated that EVs derived from human and animal semen can produce extracellular ATP, through the glycolytic pathway.^{29,30} Because proteomic analyses of HASC-EVs revealed the presence of the enzymes of the glycolysis pay-off phase (Figure 2C, Table S1), we wondered whether also HASC-EVs could produce ATP. As depicted in Figure 3A, when incubated in the presence of 5 mM glucose, both HASC-EV types produced ATP, although the amount generated by HASC-P10 was higher

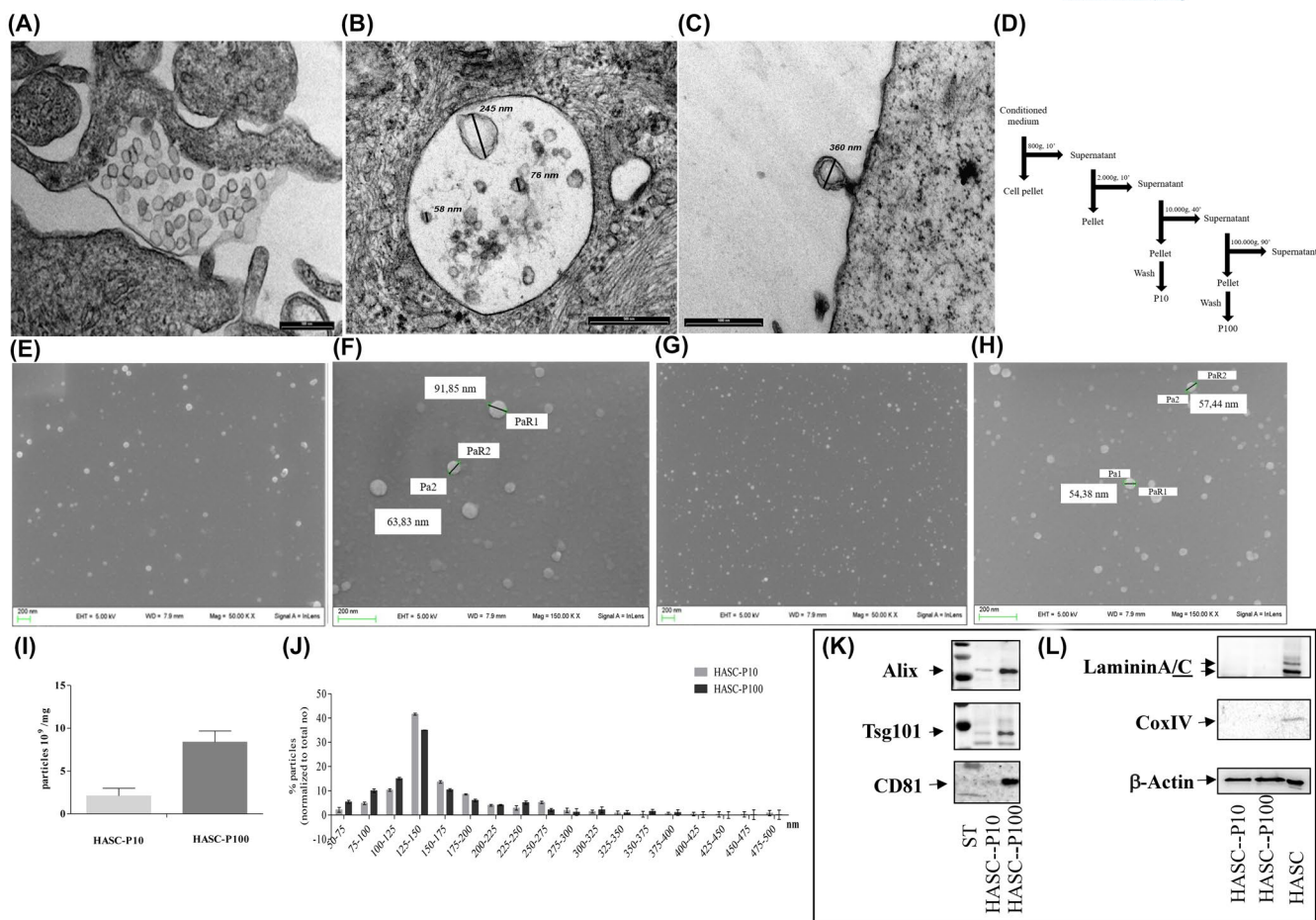


FIGURE 1 Characterization of HASC-EVs. TEM analysis of HASCs. Production of EVs by MVB (A and B) and/or ectosomes (C). (D) Flowchart of the isolation procedures by differential centrifugation. (E–H) SEM images of HASC-EVs at different magnifications, (E and F) HASC-P10, (G and H) HASC-P100. Nanoparticle tracking analysis determination of HASC-EVs concentration (I) and profile of size distribution (J). Western blotting of specific EV markers (K) and of markers characteristic of cellular organelles (L) (HASC total cell lysate was used as positive control). HASC-EVs (P10, P100) and HASCs used for western blotting analysis were from the same fresh preparation and the same amount of protein was loaded. The images and data shown are representative of one out of three independent experiments

than that of HASC-P100. Already after a 30-min incubation, both EV subsets produced a detectable amount of ATP that increased over time. Then, we addressed the localization of ATP-producing enzymes by exposing HASC-P10 and HASC-P100 to proteinase K (PK), which degrades proteins localized on EVs surface (Figure 3B). We found that PK treatment slightly reduced the amount of ATP produced by HASC-P10 while halving ATP production by HASC-P100 (Figure 3B). These data suggest that ATP production by the two EV types might involve enzymes with different localization. Furthermore, we showed that ATP production by both EV types strictly depends on the presence of exogenous ADP since its absence completely abrogated ATP production (Figure 3B). It is to highlight that ATP production was independent of the presence of exogenous NAD^+ (Figure 3B). To determine the contribution of the glycolytic pathway to ATP production, both HASC-P10 and HASC-P100 were incubated with 2-deoxy glucose (2dG), a known inhibitor

of glycolytic flux (Figure 3B). Under these experimental conditions both EV types were still capable of producing ATP, suggesting that glucose phosphorylation by hexokinase was not necessary for ATP production by EVs, thus strengthening the importance of the glycolytic pay-off phase enzymes. Due to the inefficacy of 2dG in inhibiting ATP production, we examined whether EVs could produce ATP in the absence of exogenously added glucose. We found that both HASC-P10 and HASC-P100 produced ATP under those experimental conditions (Figure 3C). Moreover, the amount of ATP produced by both EV subsets in the glucose-depleted condition was comparable. Notably, also under glucose-depleted conditions, exogenous ADP was required while NAD^+ was dispensable for ATP production (Figure 3C).

Based on these results we wondered whether other enzymes, besides the glycolytic ones, could be responsible for the sustained production of ATP under glucose-depleted conditions. It has been previously demonstrated that EVs

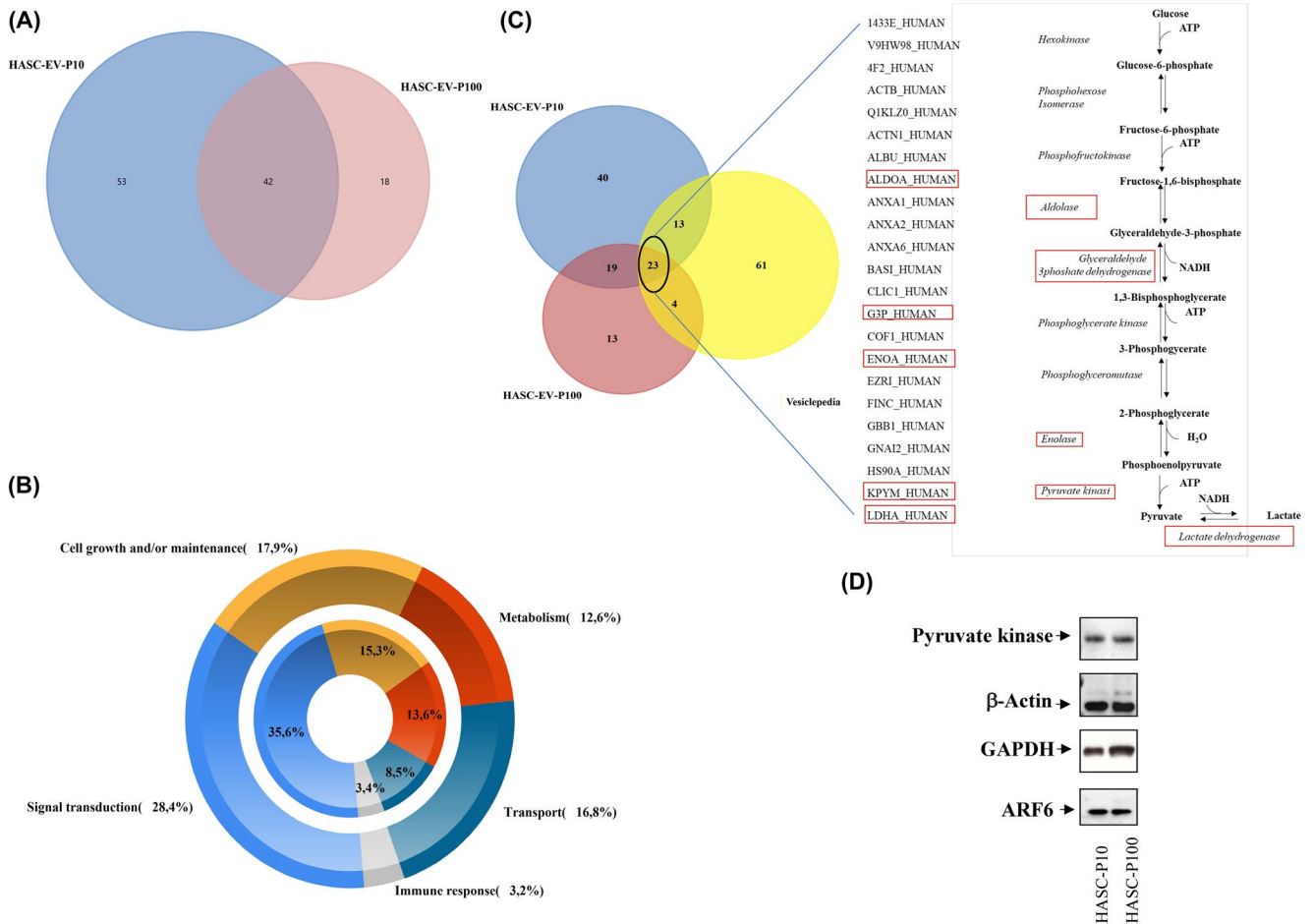


FIGURE 2 Proteomic analysis of HASC-EVs. Bioinformatic analysis of proteomics data was performed by means of FUNRICH software. (A) Venn diagram showing the overlap and differences in proteins identified in HASC- P10 and HASC- P100. (B) Comparative analysis between proteins identified in both HASC-EV subsets and Vesiclepedia database. The comparison was performed between the HASC-EVs proteins and the 100 proteins most represented in the Vesiclepedia database. The box lists EVs and Vesiclepedia common proteins. The proteins highlighted with the red boxes are enzymes of the glycolysis pay-off phase. (C) Main biological processes in which proteins identified in HASC-EVs are involved. HASC-P10 is reported on the outer chart and HASC-P100 on the inner chart. The percentage of proteins involved in the biological process is reported in brackets. (D) Western blotting validation of selected proteins identified by proteomics analysis. Results are representative of one out of three independent experiments

secreted by prostate epithelial cells can produce ATP from two ADP molecules via adenylate kinase (AK).³⁰ In order to determine whether ATP production by HASC-P10 and HASC-P100 could also be dependent on AK activity, we preincubated both types of EVs with 10 mM sodium tartrate (T) to inhibit 5'-nucleotidase. In fact, by compromising the removal of AMP by 5'-nucleotidase inhibition, the equilibrium constant of the AK reaction will be affected.³⁰ We found that in the presence of sodium tartrate (T) the amount of ATP produced by HASC-P10 was significantly reduced, whereas that of HASC-P100 resulted unaffected (Figure 3C). We then assessed the effects of rameic ions as inhibitors of GAPDH, one of the enzymes involved in the glycolysis pay-off phase. We found that the exposure to Cu^{++} prevented ATP production by HASC-P100 and significantly reduced ATP production by HASC-P10

(Figure 5C). The combination of sodium tartrate (T) and rameic ions (Cu^{++}) completely inhibited ATP production by both EVs subsets. These data suggest that AK activity contributes to ATP production by HASC-P10, whereas ATP production by HASC-P100 predominantly relies on the glycolytic pay-off phase. In order to further confirm that ATP production is related, at least in part, to the glycolysis pay-off phase, we evaluated the production of lactate. When incubated in the glycolytic reaction mixture for 30', both subsets of HASC-EVs were able to produce lactate ($310 \pm 99.0 \mu\text{M}$ and $279 \pm 83.4 \mu\text{M}$ by HASC-P10 and HASC-P100, respectively).

Besides glycolytic pay-off phase enzymes, proteomic analyses also identified 5'-nucleotidase (CD73) in both HASC-EVs types. Several reports in the literature claim the co-localization of CD73 and ectonucleoside triphosphate

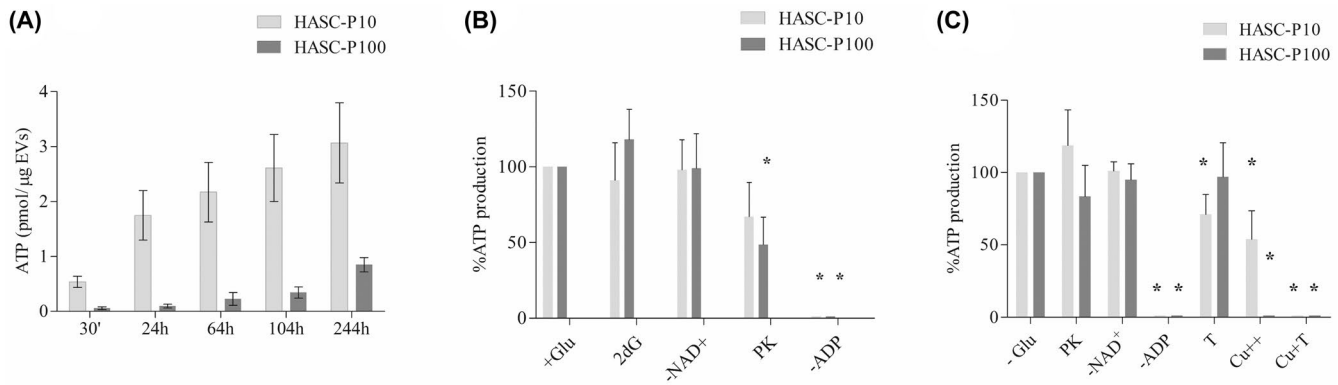


FIGURE 3 HASC-EVs are capable of producing ATP. ATP levels were measured by an ATP determination kit. (A) HASC-P10 and HASC-P100 were incubated in a glycolytic reaction mixture for the indicated time. HASC-P10 and HASC-P100 were incubated in a glycolytic reaction mixture for 30' in the presence (B) or the absence (C) of 5 mM glucose (control). The reaction mixture was supplemented with 20 mM 2-deoxyglucose (2dG), 10 mM sodium tartrate (T), 1 mM rameic sulfate (Cu^{++}) or devoided of ADP (-ADP) and NAD^+ (- NAD^+). In selected experiments, HASC-EVs were pretreated for 1 h with 50 $\mu\text{g}/\text{ml}$ proteinase K (PK) that was subsequently blocked with 2 mM PMSF. ATP levels in the presence or in the absence of glucose was assumed as 100% and used as control (HASC-P10 + Glu, 100% = 0.78 ± 0.07 pmol/ μg EVs; HASC-P100 + Glu, 100% = 0.17 ± 0.09 pmol/ μg EVs; HASC-P10 -Glu, 100% = 0.41 ± 0.25 pmol/ μg EVs; HASC-P100 - Glu, 100% = 0.13 ± 0.03 pmol/ μg EVs). HASCs were used as the positive control (ATP levels: 37.02 ± 8.0 nmol/mg of protein). Results represent the mean \pm SD of at least $n = 3$ independent experiments performed in duplicate. * $p < .05$ vs. the respective control

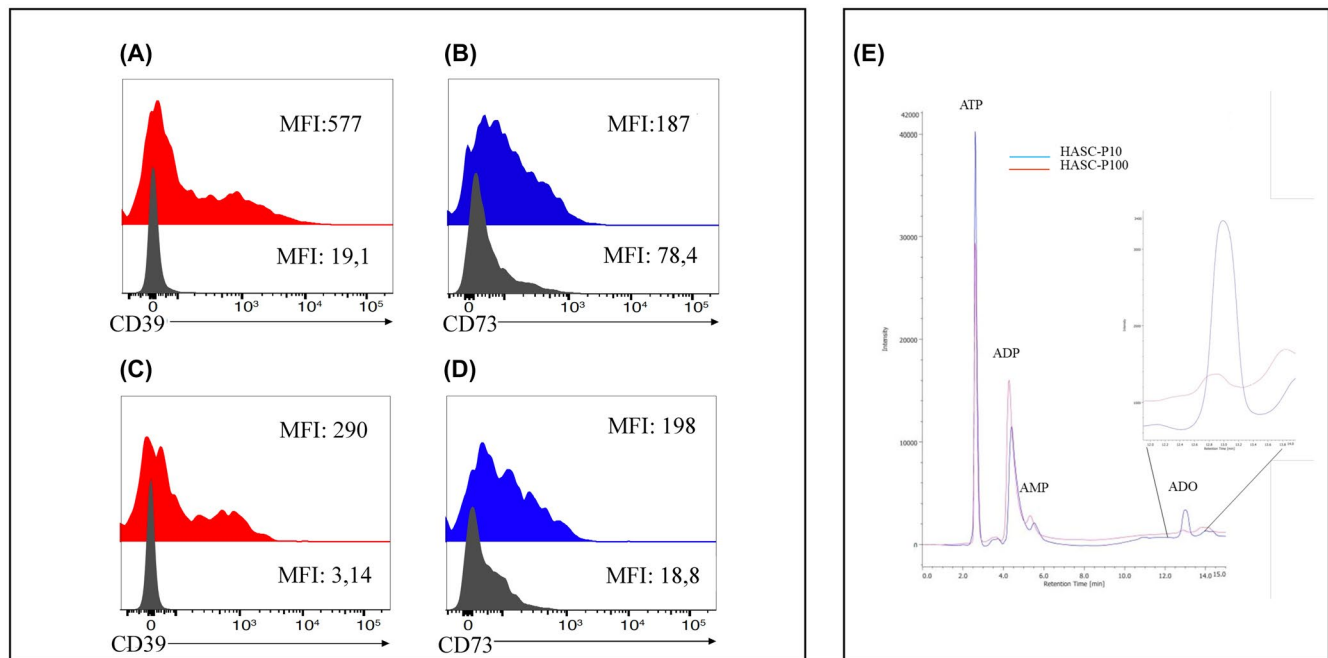


FIGURE 4 Expression of CD39 and CD73 and adenosine production in HASC-EVs. Representative flow cytometry histogram plot showing the expression level of CD39 (red) and CD73 (blue) and isotype control (grey) in HASC-P10 (A and B) and HASC-P100 (C and D). The histogram shows Mean Fluorescence Intensity (MFI) representative of one out of three independent experiments. (E) Adenosine evaluated by HPLC, representative chromatograms for the two EVs subsets is shown

diphosphohydrolase-1 (CD39) on EVs.^{25,31,32} In order to verify the presence of CD39 and CD73 on HASC-EVs, we performed a FACS analysis and, as shown in Figure 4A–D, both HASC-EV types expressed similar levels of the ectoenzymes CD39 and CD73. These data suggest that

HASC-EVs carry the enzymatic machinery for the conversion of ATP into adenosine.

To confirm our hypothesis, we incubated both HASC-EV subsets in the glycolytic buffer for 2 h and evaluated adenosine production by HPLC analysis. We found

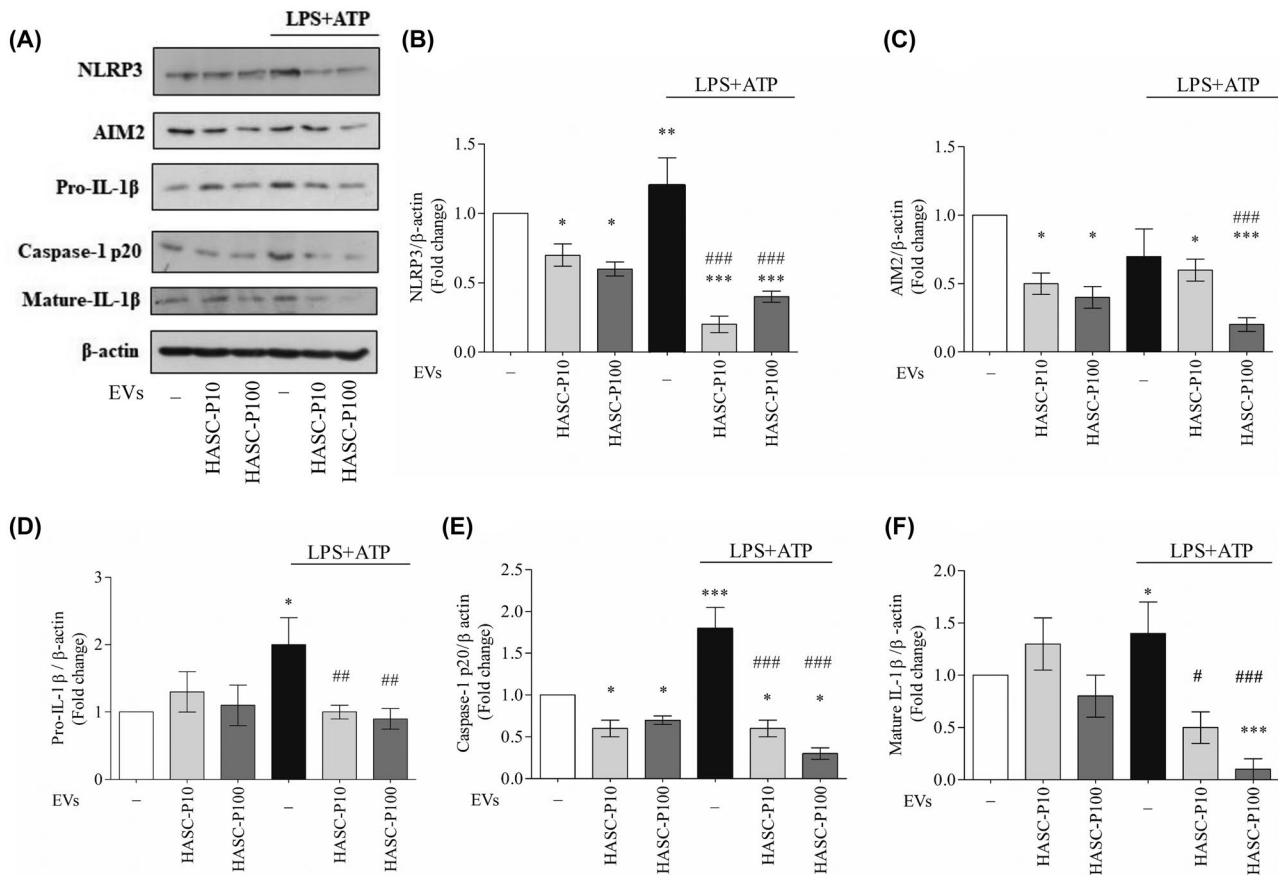


FIGURE 5 HASC-EVs prevent inflammasome activation in THP-1 cells. THP-1 cells, pre-treated for 1 h with 100 $\mu\text{g}/\text{ml}$ of HASC-P10 or HASC-P100, were subsequently primed for 20 min with 10 $\mu\text{g}/\text{ml}$ LPS and then activated for 40 min with 5 mM ATP (LPS + ATP). Cell lysates were immunoblotted with the indicated antibodies (A). β -actin was used as a loading control. Representative western blots images are shown. Histograms represent densitometric quantification (B–F) and indicate the mean \pm SD of at least $n = 3$ independent experiments each one tested in triplicate. * $p < .05$, ** $p < .01$, *** $p < .001$ vs. untreated cells. # $p < .05$, ## $p < .01$, ### $p < .001$ vs. LPS + ATP-treated cells

that both HASC-P10 and HASC-P100 produced detectable adenosine levels (Figure 4E).

3.3 | HASC-EVs prevent inflammasome activation in THP-1 cells

Our previously published data on the anti-inflammatory properties of HASC-EVs¹² along with data in the literature,²¹ prompted us to investigate whether HASC-EVs could influence the activation of NLRP3 or AIM2-inflammasome platform and IL-1 β maturation, using the human monocytic THP-1 cell line, a well-established cell model for the evaluation of inflammasome platform activation by different stimuli.^{24,33–35}

To this aim, THP-1 cells were pre-treated with either HASC-P10- or HASC-P100 (100 $\mu\text{g}/\text{ml}$) for 1 h, before being stimulated with the inflammasome activating stimuli LPS (10 $\mu\text{g}/\text{ml}$, 20 min) and ATP (5 mM, 40 min) (LPS + ATP)^{21,34,35}; control cells were left untreated or

treated with either type of EVs alone. We found that HASC-P10 or HASC-P100 pre-treatment prevented both the activation of the NLRP3/caspase-1/inflammasome platform and IL-1 β maturation after LPS and ATP treatment (Figure 5). In particular, we found that the treatment with LPS + ATP significantly increased the expression of NLRP3 (Figure 5A,B) without affecting AIM2 expression (Figure 5A,C). In the presence of LPS + ATP, HASC-EVs treatment reduced inflammasome receptors expression. In particular, HASC-P100 reduced both NLRP3 and AIM2 expression, whereas HASC-P10 only affected NLRP3. The expression levels of pro-IL-1 β , induced by LPS + ATP treatment, were significantly reduced by HASC-EVs pretreatment (Figure 5A,D). The activation of the inflammasome platform, indicated by increased expression of mature p20 Caspase-1 (Figure 5A,E) and mature IL-1 β (Figure 5A,F), by LPS + ATP treatment was completely abolished in the presence of HASC-EVs. These data indicate that HASC-EVs regulate inflammatory responses

in THP-1 cells, suggesting an anti-inflammatory potential for HASC-EVs.

To gain insights into the mechanism by which HASC-EVs prevented inflammasome activation in THP-1 cells, HASC-P10 and HASC-P100 were labeled with DiI and then incubated with THP1 cells to check their potential interaction. FACS analysis showed a $17.5 \pm 2.2\%$ and a $15.3 \pm 3.0\%$ of DiI positive THP-1 cells after exposure to HASC-P10 and HASC-P100, respectively (Figure 6A,C,E), indicating some degree of uptake/interaction between EVs and THP-1 cells. To define whether a protein–protein-mediated interaction occurred between THP-1 cells and EVs, we performed crosslinking experiments using BS(PEG)5. Nevertheless, treatment with the crosslinking agent (CL) did not further increase the percentage of DiI-positive THP-1 cells (Figure 6B,D,F). To understand whether the fluorescence signal detected by the FACS analysis was correlated with the internalization of the EVs or if was confined outside the cell, we analyzed THP-1 cells exposed to HASC-EVs by fluorescence microscopy. The images show that fluorescence is predominantly external

to the cells for both EVs types (Figure 6G,H). These data indicate that THP-1 cells do not uptake HASC-EVs.

3.4 | HASC-EVs anti-inflammatory effects rely on adenosine A2a receptor

The ability of HASC-EVs to produce adenosine, an important modulator of inflammation^{30,36} led us to hypothesize that adenosine receptor activation might be involved in inflammasome inhibition in THP-1 cells.

To address this hypothesis, we used NECA a high-affinity non-selective adenosine receptor agonist, and found that, similarly to HASC-EVs, pre-treatment of THP-1 cells with NECA for 1 h completely prevented caspase-1 activation induced by LPS and ATP (Figure 7A,B), suggesting the involvement of an adenosine receptor subtype in Caspase-1 modulation. We then preincubated THP-1 cells with CGS-21680, a selective A2a adenosine receptor agonist, and found it abolished Caspase-1 activation (Figure 7C,D), indicating that A2a adenosine receptor

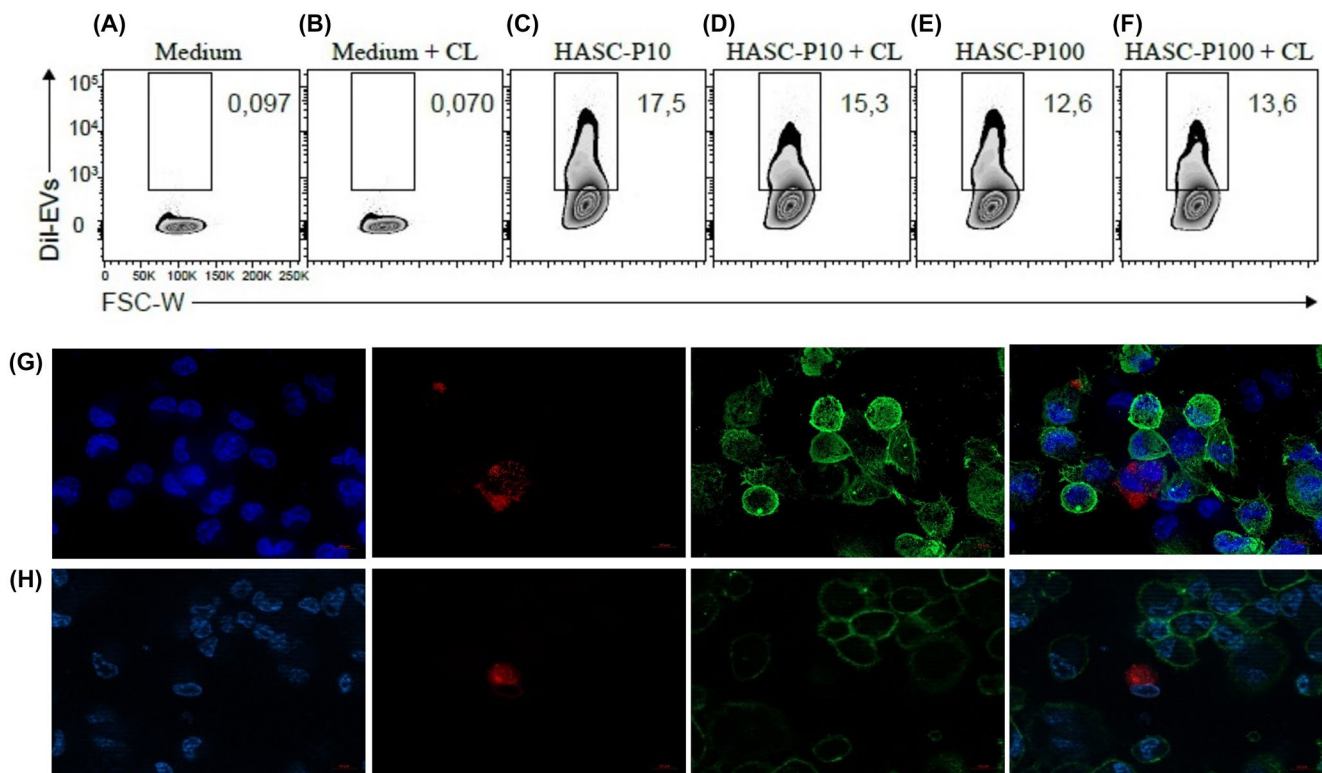


FIGURE 6 THP-1 cells do not uptake HASC-EVs. THP-1 cells were treated with DiI-labeled HASC-P10 and HASC-P100 and analyzed by flow cytometry. Chemical crosslink (CL) was performed with BS(PEG)5. The sequence of flow cytometry histogram plot was: (A) THP-1 cells in basal medium, (B) THP-1 cells in basal medium plus the crosslinking agent, (C) THP-1 cells exposed to labeled HASC-P10, (D) THP-1 cells exposed to labeled HASC-P10 with chemical crosslink, (E) THP-1 cells exposed to labeled HASC-P100, (F) THP-1 cells exposed to labeled HASC-P100 with chemical crosslink. Intracellular localization of EVs. THP-1 cells were exposed to DiI-stained HASC-EVs (HASC-P10 [G]; HASC-P100 [H]) for 2 h and then fixed with 4% PFA. The cell membrane was stained with CellMask™ Green Plasma Membrane Stain and nuclei were counterstained with DAPI. The images are representative of one out of three separate experiments. Magnification 63×

activation is involved in Caspase-1 regulation. It is to note that none of the treatments affected adenosine A2a receptor expression in THP-1 cells (Figure 7E,F).

To confirm the involvement of the adenosine A2a receptor on HASC-EVs-mediated inhibition of inflammasome activation, we pretreated THP-1 cells with the selective adenosine A2a receptor antagonist ZM-241385. As shown in Figure 8, the adenosine A2a receptor antagonist completely prevented HASC-EVs effect on caspase-1 (Figure 8A,C), without affecting NLRP3 protein expression (Figure 8A,B). Adenosine A2a receptor activation culminates in the activation of cAMP-dependent protein kinase (PKA) which is known to phosphorylate NLRP3 at Ser295, thus leading to an inflammasome platform disassembly.³⁷ We found that the exposure of THP-1 cells to both EV subsets, in the presence of LPS + ATP, increased NLRP3 phosphorylation (Figure 8D,E) and decreased ASC polymerization, as evidenced by crosslinking experiment (Figure 8F). Moreover, pretreatment with ZM-241385 reverted EVs induced effects on ASC polymerization (Figure 8F). Altogether these data demonstrate that both HASC-P10 and HASC-P100 suppress inflammasome signaling in THP-1 via adenosine release and adenosine A2a receptor activation, leading to NLRP3 phosphorylation and blockade of caspase-1 activation.

4 | DISCUSSION

Our results demonstrate for the first time that HASC-EVs possess intrinsic metabolic activities, whose products influence the inflammatory behavior of monocytic THP-1 cells. Specifically, we have shown that HASC-EVs are capable of producing adenosine which, acting as a soluble mediator, activates adenosine A2a receptor leading to inhibition of NLRP3 inflammasome platform assembly.

EV purification by differential centrifugation led to the isolation of two distinct EV subsets namely HASC-P10 and HASC-P100. According to MISEV2014 guidelines, a potential bias in the EVs isolation procedure is the separation of non-vesicular entities from EVs. MISEV2018 guidelines³⁸ highlighted that, besides this concern is still valid, isolation by differential ultracentrifugation can result in an intermediate recovery and intermediate specificity. In fact, we found that mitochondrial or nuclear proteins were not detected in HASC-EVs preparations. It is to underline that, according to MISEV 2018 guidelines, we isolated EVs from culture media deprived of FBS thus further reducing the potential carryover of contaminant serum-derived proteins and lipoproteins. Nonetheless, the carryover of contaminants cannot be excluded. The isolated HASC-P10 and HASC-P100 are characterized by the same dimensional range but different sedimentation

rates. Several reports link the dimensional differences to density characteristics.^{39,40} Here, we showed that, despite a distinct sedimentation rates, the two HASC- EV subsets were characterized by comparable mean diameter, suggesting that they have a different composition of biological molecules. Furthermore, our data highlight that both EV subsets achieve the same functional effects but use only partially overlapping mechanisms.

The immunomodulatory effects of mesenchymal stem cells (MSCs) and their secretory products have been largely explored in recent years^{41,42} and it has been shown that EVs play a crucial role in the stem cell secretome functions.^{3,12,41,43} In addition, MSC-EVs contain bioactive molecules that are able to regulate the phenotype, function, and homing of immune cells.³

Inflammasomes are molecular platforms activated upon cellular infection or stress that trigger the maturation of proinflammatory cytokines to engage innate immune defenses. Inflammasome activation leads to caspase-1 activation, which in turn culminates in the maturation and secretion of IL-1 β and IL-18.⁴⁴ IL-1 family has numerous activities that are important for adaptive immune responses.⁴⁵ We have already demonstrated that HASCs release EVs containing immunoregulatory molecules capable of modifying the phenotype of T lymphocytes.¹² Here, we aimed at examining whether HASC-EVs were capable of interfering with inflammasome activation, a master player in inflammatory and immune responses.^{46,47} In agreement with data in the literature, our results demonstrate that HASC-EVs play a pivotal role in negatively modulating inflammasome activation.⁴⁸⁻⁵¹ Rajan et al. showed that human periodontal ligament stem cell-derived exosomes could negatively modulate NALP3 inflammasome activation,⁵² while Zhang et al.⁵³ demonstrated how MSC-derived exosomes reduce inflammatory processes by dampening the release of IL-1 β . Our results, obtained in an in vitro model of inflammasome activation, demonstrated that THP-1 cells conditioned with HASC-EVs failed to activate NLRP3/caspase-1/inflammasome platform and IL-1 β maturation in response to LPS + ATP treatment. Indeed, inflammasome activation requires two stimuli: LPS which increases the expression of inflammasome cascade components, and ATP which, through P2X7 purinergic receptor, induces the assembly of the inflammasome platform.¹⁸

In particular, we found that, through a molecular mechanism that induces NALP3 phosphorylation, the inflammasome platform did not assemble when THP-1 cells are pretreated with HASC- EVs.

Surprisingly, the achievement of these biological results depended neither on the release of vesicle content into THP-1 cells nor on membrane-membrane contact between vesicles and cells. In fact, flow cytometric and

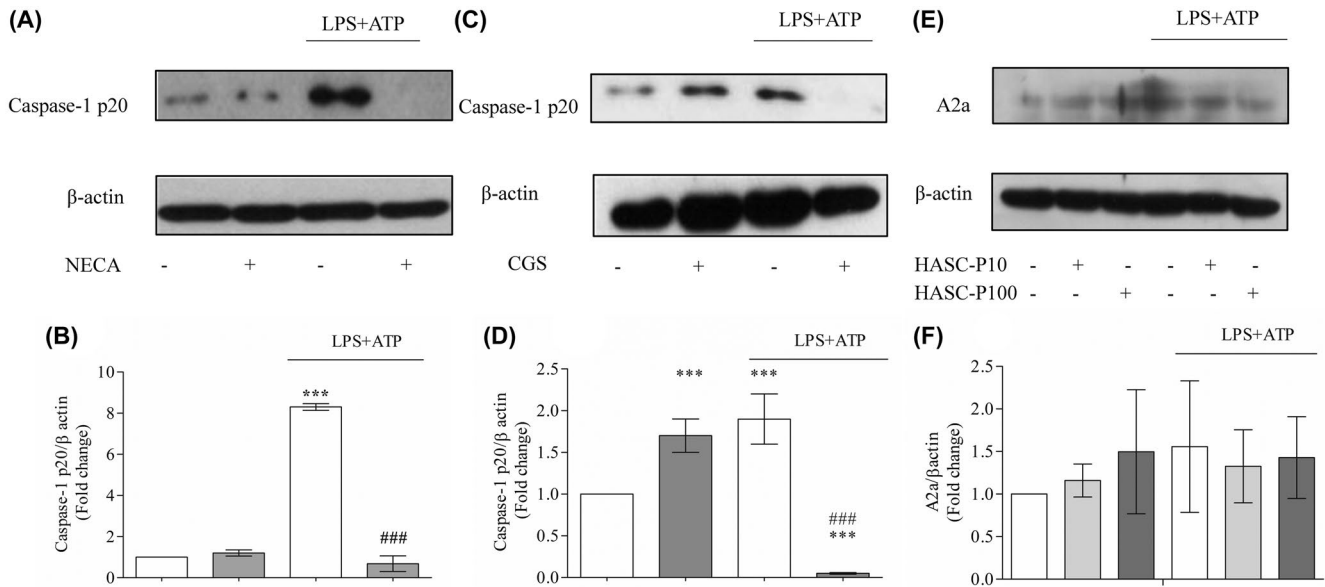


FIGURE 7 HASC-EVs anti-inflammatory effects rely on adenosine A2a receptor. THP-1 cells were pretreated for 1 h with 1 μ M NECA (A and B) or 100 μ M CGS-21680 (C and D) subsequently primed for 20 min with 10 μ g/ml LPS and then activated for 40 min with 5 mM ATP (LPS + ATP). Cell lysates were immunoblotted for Caspase-1. THP-1 cells were pre-treated for 1 h with 100 μ g/ml of HASC-P10 or HASC-P100, subsequently primed for 20 min with 10 μ g/ml LPS and then activated for 40 min with 5mM ATP (LPS + ATP). Cell lysates were immunoblotted for adenosine A2a receptor (E and F). β -actin was used as a loading control. Representative western blots images are shown. Histograms represent densitometric quantification and indicate the mean \pm SD of at least $n = 3$ independent experiments each one tested in triplicate. *** $p < .001$ vs. untreated cells. ### $p < .001$ vs. LPS + ATP treated cells

microscopy analyses indicated that these cells did not take up nor exerted a protein-protein-mediated interaction with HASC-EVs. An alternative way by which EVs may condition THP-1 cells foresees the production of soluble factors. We hypothesized that HASC-EVs could release soluble factors related to their specific enzymatic activity. In fact, the analysis of the HASC-EVs proteome revealed the presence of glycolytic enzymes, in particular the enzymes of the pay-off phase which led to ATP production. This result is in agreement with findings by Ronquist and collaborators demonstrating the presence of glycolytic enzymes capable of producing ATP on EVs isolated from prostate cancer cells.^{29,30} Moreover, HASC-EVs also carry CD39 and CD73, which are capable of converting ATP into AMP and AMP into adenosine, respectively.

Data in the literature report that the enzymatic activities of CD39 and CD73 play strategic roles in calibrating the duration, magnitude, and chemical nature of purinergic signals delivered to immune cells through the conversion of ATP into adenosine. This drives a shift from an ATP-driven proinflammatory environment to an anti-inflammatory milieu induced by adenosine.⁵⁴ Adenosine plays a key role in modulating inflammatory responses. In fact, it has been demonstrated that extracellular adenosine prevents excessive inflammation by suppressing proinflammatory cytokine production.^{55–58} However, reports in the literature claim both

pro-inflammatory and anti-inflammatory effects for both ATP and adenosine. It is conceivable that the final effect of ATP and adenosine on the immune response depends on the balance between ATP and adenosine in the immediate vicinity of the cells.^{36,55} Adenosine exerts its anti-inflammatory effects through four cell-surface G-protein coupled adenosine receptors subtypes, namely A1, A2a, A2b, and A3. Adenosine receptors have different sensitivities to nucleoside concentration so that A1 and A2a are activated by low levels of adenosine, whereas A2b and A3 require higher ligand amount.⁵⁹ As several lines of research suggested, adenosine may mediate anti-inflammatory effects via the stimulation of the A2a adenosine receptor.^{60–64} Adenosine A2a receptor is a stimulatory G-protein coupled receptor whose activation leads to the accumulation of intracellular cAMP. This compound subsequently activates the cAMP-dependent protein kinase (PKA).⁶⁵ It has been thoroughly demonstrated that protein kinase-mediated phosphorylation of NLRP3 at Ser 295 exerts inhibitory effects on inflammasome activation by impeding platform assembly^{24,37,66} and that PKA is deeply involved in the process.⁶⁶ Our results support the hypothesis that, upon adenosine A2a receptor engagement, PKA activation mediates the phosphorylation of NLRP3 inflammasome receptor at Ser 295 thus impeding ASC oligomerization, indicative of inflammasome platform

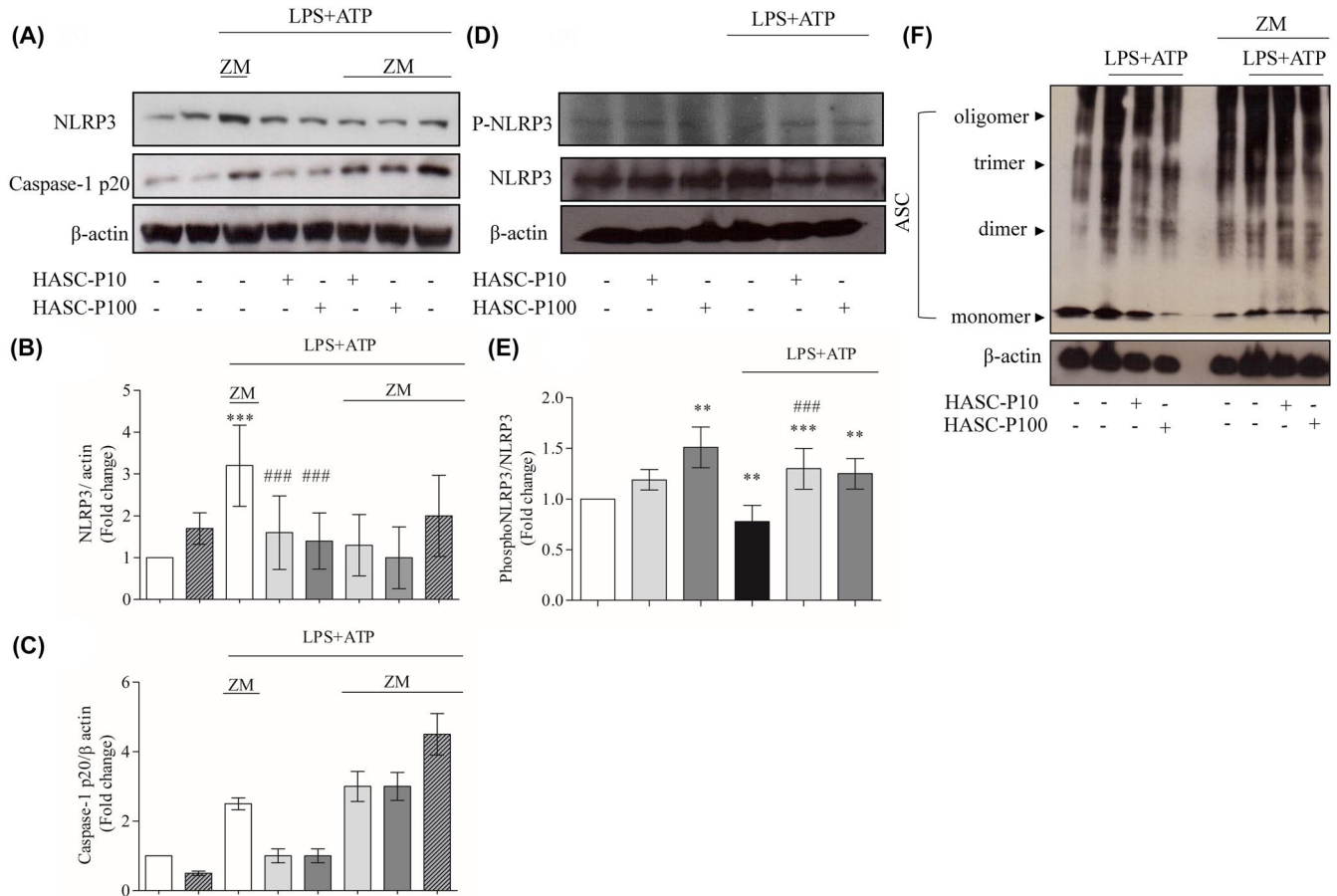


FIGURE 8 HASC-EVs affect inflammasome assembly via A2a receptor engagement. THP-1 cells were pre-treated for 1 h with 100 μ g/ml of HASC-P10 or HASC-P100, subsequently primed for 20 min with 10 μ g/ml LPS and then activated for 40 min with 5 mM ATP (LPS + ATP). In selected experiments ZM-241385 (500 nM) was added 1 h before HASC-P10 or HASC-P100 treatment; cell lysates were immunoblotted for NLRP3 (A,B), Caspase-1 (A,C), p-NLRP3 (Ser295) (D and E). ASC oligomerization was assessed by crosslinking assay followed by Western blot analysis (F). The blots were stripped and re-probed with mouse anti- β -actin, to confirm equal loading. Representative western blots images are shown. Histograms represent densitometric quantification and indicate the mean \pm SD of at least $n = 3$ independent experiments each one tested in triplicate. ** $p < .01$, *** $p < .001$ vs. untreated cells; ### $p < .01$, #### $p < .001$ vs. LPS + ATP treated cells

assembly. Confirmation of adenosine A2a receptor involvement was given by the use of a specific agonist and antagonist. CGS-21680, a specific adenosine A2a receptor agonist, exerts superimposable effects on HASC-EVs, whereas the EVs effects were reversed when ZM-241385, an adenosine A2a receptor antagonist, was co-administered.

In conclusion, we have demonstrated that HASC-EVs exert immunomodulatory effects on THP-1 cells by dampening inflammasome activation (Figure 9). It must be highlighted that these effects seem not to depend on the physical interaction between EVs and recipient cells, but to be mediated by the production of soluble mediators by EVs themselves. It is worth noting that both types of HASC-EVs produce ATP, but through only partially overlapping biochemical processes. In fact, the data obtained in our experimental conditions suggest that both

EVs types use glycolysis pay-off phase enzyme, but that in the HASC-P10 subset also adenylate kinase plays an important role.

These results offer a new point of view on the role of EVs, in fact, they can be considered not just mere transporters of pre-formed biomolecules, but also subcellular particles capable of playing an active role in microenvironment homeostasis via the autonomous synthesis of soluble metabolic products which, by altering tissue microenvironment composition, can affect cellular behaviors.

ACKNOWLEDGMENTS

This study has been funded by the Department of Experimental Medicine, University of Perugia, Basic Research to IB. The authors thank Francesco Fabi for the technical assistance and Dr. Lara Macchioni for performing experiments for the revised version.

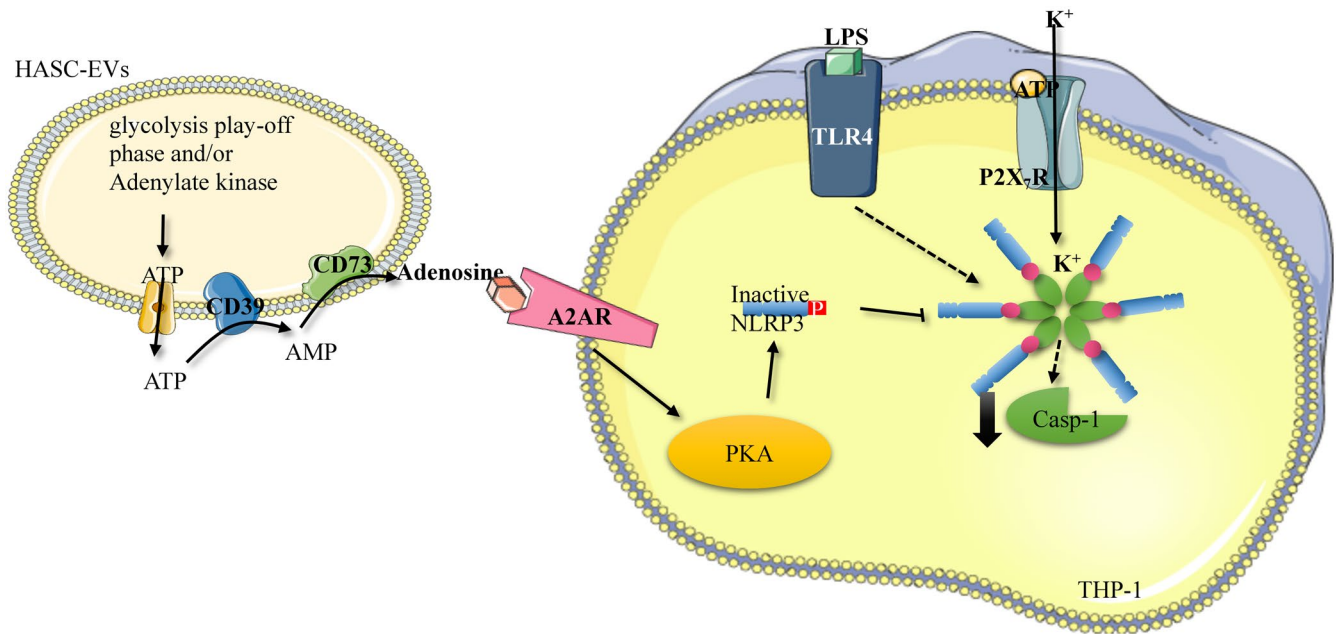


FIGURE 9 Proposed diagram of possible interaction between HASC-EVs and THP-1 cells. HASC-EVs autonomously produce ATP via the glycolysis pay-off phase and, at least in part, through adenylate kinase activity. HASC-EVs, through their CD39 and CD75 activities, convert ATP into Adenosine which acts as an agonist for the A2a adenosine receptor on THP-1 cells. Being A2a a stimulatory G-protein-coupled receptor, its engagement leads to the activation of protein kinase A (PKA) that phosphorylates NLRP3 at Ser295. This event impedes inflammasome platform assembly leading to a reduction in active caspase-1 and mature IL-1 β

DISCLOSURES

The authors declare that there is no conflict of interest.

AUTHOR CONTRIBUTIONS

Letizia Mezzasoma, Ilaria Bellezza, Vincenzo Nicola Talesa, Francesca Fallarino and Rita Romani designed research; Letizia Mezzasoma, Ilaria Bellezza, Pierluigi Orvietani, Giorgia Manni, Marco Gargaro, Rita Romani performed research; Krizia Sagini, Alicia Llorente, Paolo Scarpelli, Luisa Pascucci, Barbara Cellini contributed analytic tools and performed some experiments; Letizia Mezzasoma, Ilaria Bellezza, and Rita Romani wrote the manuscript; All authors were involved in revising the manuscript.

DATA AVAILABILITY STATEMENT

The data that support the findings of this study are available from the corresponding author upon reasonable request.

ORCID

Letizia Mezzasoma <https://orcid.org/0000-0002-6159-0927>
 Ilaria Bellezza <https://orcid.org/0000-0002-8106-1600>
 Giorgia Manni <https://orcid.org/0000-0002-5697-2648>
 Marco Gargaro <https://orcid.org/0000-0003-0645-9800>
 Krizia Sagini <https://orcid.org/0000-0003-3357-2171>
 Alicia Llorente <https://orcid.org/0000-0002-0045-071X>
 Paolo Scarpelli <https://orcid.org/0000-0001-6583-3693>
 Luisa Pascucci <https://orcid.org/0000-0002-2562-1140>

Barbara Cellini <https://orcid.org/0000-0002-5221-9288>
 Francesca Fallarino <https://orcid.org/0000-0002-8501-2136>
 Rita Romani <https://orcid.org/0000-0003-2612-9796>

REFERENCES

- Théry C, Zitvogel L, Amigorena S. Exosomes: composition, biogenesis and function. *Nat Rev Immunol*. 2002;2(8):569-579. doi:10.1038/nri855
- Bebelmann MP, Smit MJ, Pegtel DM, Baglio SR. Biogenesis and function of extracellular vesicles in cancer. *Pharmacol Ther*. 2018;188:1-11. doi:10.1016/j.pharmthera.2018.02.013
- Harrell CR, Jovicic N, Djonov V, Arsenijevic N, Volarevic V. Mesenchymal stem cell-derived exosomes and other extracellular vesicles as new remedies in the therapy of inflammatory diseases. *Cells*. 2019;8(12):1605. doi:10.3390/cells8121605
- Keshtkar S, Azarpira N, Ghahremani MH. Mesenchymal stem cell-derived extracellular vesicles: novel frontiers in regenerative medicine. *Stem Cell Res Ther*. 2018;9(1):63. doi:10.1186/s13287-018-0791-7
- Todorova D, Simoncini S, Lacroix R, Sabatier F, Dignat-George F. Extracellular vesicles in angiogenesis. *Circ Res*. 2017;120(10):1658-1673. doi:10.1161/CIRCRESAHA.117.309681
- Veerman RE, Akpınar GG, Eldh M, Gabriëlsson S. Immune cell-derived extracellular vesicles—functions and therapeutic applications. *Trends Mol Med*. 2019;25(5):382-394.
- McKelvey KJ, Powell KL, Ashton AW, Morris JM, McCracken SA. Exosomes: mechanisms of uptake. *J Circ Biomark*. 2015;4:7.
- Zhang X, Yuan X, Shi H, Wu L, Qian H, Xu W. Exosomes in cancer: small particle, big player. *J Hematol Oncol*. 2015;8(1):1-13.

9. Iraci N, Gaude E, Leonardi T, et al. Extracellular vesicles are independent metabolic units with asparaginase activity. *Nat Chem Biol.* 2017;13(9):951-955.
10. Garcia NA, Moncayo-Arlandi J, Sepulveda P, Diez-Juan A. Cardiomyocyte exosomes regulate glycolytic flux in endothelium by direct transfer of GLUT transporters and glycolytic enzymes. *Cardiovasc Res.* 2016;109(3):397-408.
11. Ronquist KG, Ek B, Stavreus-Evers A, Larsson A, Ronquist G. Human prostates express glycolytic enzymes with capacity for ATP production. *Am J Physiol Endocrinol Metab.* 2013;304(6):E576-E582.
12. Romani R, Pirisinu I, Calvitti M, et al. Stem cells from human amniotic fluid exert immunoregulatory function via secreted indoleamine 2, 3-dioxygenase1. *J Cell Mol Med.* 2015;19(7):1593-1605.
13. Zhu YU, Wang Y, Zhao B, et al. Comparison of exosomes secreted by induced pluripotent stem cell-derived mesenchymal stem cells and synovial membrane-derived mesenchymal stem cells for the treatment of osteoarthritis. *Stem Cell Res Ther.* 2017;8(1):1-11.
14. Caplan AI, Dennis JE. Mesenchymal stem cells as trophic mediators. *J Cell Biochem.* 2006;98(5):1076-1084.
15. Nojehdehi S, Soudi S, Hesampour A, Rasouli S, Soleimani M, Hashemi SM. Immunomodulatory effects of mesenchymal stem cell-derived exosomes on experimental type-1 autoimmune diabetes. *J Cell Biochem.* 2018;119(11):9433-9443.
16. Shigemoto-Kuroda T, Oh JY, Kim D-K, et al. MSC-derived extracellular vesicles attenuate immune responses in two autoimmune murine models: type 1 diabetes and uveoretinitis. *Stem Cell Reports.* 2017;8(5):1214-1225.
17. Mariathasan S, Monack DM. Inflammasome adaptors and sensors: intracellular regulators of infection and inflammation. *Nat Rev Immunol.* 2007;7(1):31-40.
18. Rathinam VA, Vanaja SK, Fitzgerald KA. Regulation of inflammasome signaling. *Nat Immunol.* 2012;13(4):333-342.
19. Martinon F, Tschopp J. Inflammatory caspases: linking an intracellular innate immune system to autoinflammatory diseases. *Cell.* 2004;117(5):561-574.
20. Kelley N, Jeltema D, Duan Y, He Y. The NLRP3 inflammasome: an overview of mechanisms of activation and regulation. *Int J Mol Sci.* 2019;20(13):3328.
21. Mezzasoma L, Costanzi E, Scarpelli P, Talesa VN, Bellezza I. Extracellular vesicles from human advanced-stage prostate cancer cells modify the inflammatory response of microenvironment-residing cells. *Cancers.* 2019;11(9):1276.
22. Chiasserini D, Davidescu M, Orvietani PL, et al. 3-Bromopyruvate treatment induces alterations of metabolic and stress-related pathways in glioblastoma cells. *J Proteomics.* 2017;152:329-338.
23. Fonseka P, Pathan M, Chitti SV, Kang T, Mathivanan S. FunRich enables enrichment analysis of OMICS datasets. *J Mol Biol.* 2021;433(11):166747.
24. Mezzasoma L, Talesa VN, Romani R, Bellezza I. ANP and BNP exert anti-inflammatory action via NPR-1/cGMP axis by interfering with canonical, non-canonical, and alternative routes of inflammasome activation in human THP1 cells. *Int J Mol Sci.* 2021;22(1):24.
25. Bjørge I, Kim S, Mano J, Kalionis B, Chrzanowski W. Extracellular vesicles, exosomes and shedding vesicles in regenerative medicine—a new paradigm for tissue repair. *Biomater Sci.* 2018;6(1):60-78.
26. O'Connell JS, Lee C, Farhat N, et al. Administration of extracellular vesicles derived from human amniotic fluid stem cells: a new treatment for necrotizing enterocolitis. *Pediatr Surg Int.* 2021;37:1-9. doi:10.1007/s00383-020-04826-6
27. Takov K, He Z, Johnston HE, et al. Small extracellular vesicles secreted from human amniotic fluid mesenchymal stromal cells possess cardioprotective and promigratory potential. *Basic Res Cardiol.* 2020;115(3):26. doi:10.1007/s00395-020-0785-3
28. Balbi C, Piccoli M, Barile L, et al. First characterization of human amniotic fluid stem cell extracellular vesicles as a powerful paracrine tool endowed with regenerative potential. *Stem Cells Transl Med.* 2017;6:1340-1355. doi:10.1002/sctm.16-0297
29. Ronquist KG, Sanchez C, Dubois L, et al. Energy-requiring uptake of prostates and PC3 cell-derived exosomes into non-malignant and malignant cells. *J Extracell Vesicles.* 2016;5(1):29877.
30. Ronquist KG, Ek BO, Morrell J, et al. Prostates from four different species are able to produce extracellular adenosine triphosphate (ATP). *Biochim Biophys Acta.* 2013;1830(10):4604-4610.
31. Angioni R, Liboni C, Herkenne S, et al. CD73+ extracellular vesicles inhibit angiogenesis through adenosine A2B receptor signalling. *J Extracell Vesicles.* 2020;9(1):1757900.
32. Clayton A, Al-Taei S, Webber J, Mason MD, Tabi Z. Cancer exosomes express CD39 and CD73, which suppress T cells through adenosine production. *J Immunol.* 2011;187(2):676-683.
33. Campden RI, Warren AL, Greene CJ, et al. Extracellular cathepsin Z signals through the $\alpha 5$ integrin and augments NLRP3 inflammasome activation. *J Biol Chem.* 2021;298(1):101459.
34. Mezzasoma L, Antognelli C, Talesa VN. A novel role for brain natriuretic peptide: inhibition of IL-1 secretion via downregulation of NF-kB/Erk 1/2 and NALP3/ASC/Caspase-1 activation in human THP-1 monocyte. *Mediators Inflamm.* 2017;2017:5858315.
35. Mezzasoma L, Antognelli C, Talesa VN. Atrial natriuretic peptide down-regulates LPS/ATP-mediated IL-1 β release by inhibiting NF-kB, NLRP3 inflammasome and caspase-1 activation in THP-1 cells. *Immunol Res.* 2016;64(1):303-312.
36. Ratajczak MZ, Kucia M. Extracellular adenosine triphosphate (eATP) and its metabolite, extracellular adenosine (eAdo), as opposing “Yin-Yang” regulators of Nlrp3 inflammasome in the trafficking of hematopoietic stem/progenitor cells. *Front Immunol.* 2020;11:603942.
37. Poli G, Fabi C, Bellet MM, et al. Epigenetic mechanisms of inflammasome regulation. *Int J Mol Sci.* 2020;21(16):5758.
38. Théry C, Witwer KW, Aikawa E, et al. Minimal information for studies of extracellular vesicles 2018 (MISEV2018): a position statement of the International Society for Extracellular Vesicles and update of the MISEV2014 guidelines. *J Extracell Vesicles.* 2018;7(1):1535750.
39. Chen B-Y, Sung C-H, Chen C, et al. Advances in exosomes technology. *Clin Chim Acta.* 2019;493:14-19.
40. Taylor DD, Shah S. Methods of isolating extracellular vesicles impact down-stream analyses of their cargoes. *Methods.* 2015;87:3-10.
41. Harrell CR, Fellabaum C, Jovicic N, Djonov V, Arsenijevic N, Volarevic V. Molecular mechanisms responsible for therapeutic

- potential of mesenchymal stem cell-derived secretome. *Cells*. 2019;8(5):467.
42. Lin L, Du L. The role of secreted factors in stem cells-mediated immune regulation. *Cell Immunol*. 2018;326:24-32.
 43. Phinney DG, Pittenger MF. Concise review: MSC-derived exosomes for cell-free therapy. *Stem Cells*. 2017;35(4):851-858.
 44. Schroder K, Tschopp J. The inflammasomes. *Cell*. 2010;140(6):821-832.
 45. Garlanda C, Dinarello CA, Mantovani A. The interleukin-1 family: back to the future. *Immunity*. 2013;39(6):1003-1018.
 46. Biasizzo M, Kopitar-Jerala N. Interplay between NLRP3 inflammasome and autophagy. *Front Immunol*. 2020;11:2470.
 47. Rathinam VA, Fitzgerald KA. Inflammasome complexes: emerging mechanisms and effector functions. *Cell*. 2016;165(4):792-800.
 48. Jiang L, Zhang S, Hu H, et al. Exosomes derived from human umbilical cord mesenchymal stem cells alleviate acute liver failure by reducing the activity of the NLRP3 inflammasome in macrophages. *Biochem Biophys Res Comm*. 2019;508(3):735-741.
 49. Liu Y, Lou G, Li A, et al. AMSC-derived exosomes alleviate lipopolysaccharide/d-galactosamine-induced acute liver failure by miR-17-mediated reduction of TXNIP/NLRP3 inflammasome activation in macrophages. *EBioMedicine*. 2018;36:140-150.
 50. Zeng Q, Zhou Y, Liang D, et al. Exosomes secreted from bone marrow mesenchymal stem cells attenuate oxygen-glucose deprivation/reoxygenation-induced pyroptosis in PC12 cells by promoting AMPK-dependent autophagic flux. *Front Cell Neurosci*. 2020;14:182.
 51. Zhang W, Wang Y, Kong Y. Exosomes derived from mesenchymal stem cells modulate miR-126 to ameliorate hyperglycemia-induced retinal inflammation via targeting HMGB1. *Invest Ophthalmol Vis Sci*. 2019;60(1):294-303.
 52. Soundara Rajan T, Giacoppo S, Diomedea F, Bramanti P, Trubiani O, Mazzon E. Human periodontal ligament stem cells secretome from multiple sclerosis patients suppresses NALP3 inflammasome activation in experimental autoimmune encephalomyelitis. *Int J Immunopathol Pharmacol*. 2017;30(3):238-252.
 53. Zhang S, Teo KYW, Chuah SJ, Lai RC, Lim SK, Toh WS. MSC exosomes alleviate temporomandibular joint osteoarthritis by attenuating inflammation and restoring matrix homeostasis. *Biomaterials*. 2019;200:35-47.
 54. Antonioli L, Pacher P, Vizi ES, Haskó G. CD39 and CD73 in immunity and inflammation. *Trends Mol Med*. 2013;19(6):355-367.
 55. Faas M, Sáez T, De Vos P. Extracellular ATP and adenosine: the Yin and Yang in immune responses? *Mol Aspects Med*. 2017;55:9-19.
 56. Haskó G, Németh ZH, Vizi ES, Salzman AL, Szabó C. An agonist of adenosine A3 receptors decreases interleukin-12 and interferon- γ production and prevents lethality in endotoxemic mice. *Eur J Pharmacol*. 1998;358(3):261-268.
 57. Haskó G, Cronstein BN. Adenosine: an endogenous regulator of innate immunity. *Trends Immunol*. 2004;25(1):33-39.
 58. Okusa MD, Linden J, Huang L, Rieger JM, Macdonald TL, Huynh LP. A2A adenosine receptor-mediated inhibition of renal injury and neutrophil adhesion. *Am J Physiol Renal Physiol*. 2000;279(5):F809-F818.
 59. Morello S, Sorrentino R, Pinto A. Adenosine A2a receptor agonists as regulators of inflammation: pharmacology and therapeutic opportunities. *J Receptor Ligand Channel Res*. 2009;2:11-17.
 60. Haskó G, Pacher P. A2A receptors in inflammation and injury: lessons learned from transgenic animals. *J Leukoc Biol*. 2008;83(3):447-455.
 61. Lappas CM, Sullivan GW, Linden J. Adenosine A2A agonists in development for the treatment of inflammation. *Expert Opin Investig Drugs*. 2005;14(7):797-806.
 62. Palmer T, Trevethick M. Suppression of inflammatory and immune responses by the A2A adenosine receptor: an introduction. *Br J Pharmacol*. 2008;153(S1):S27-S34.
 63. Sitkovsky MV. Use of the A2A adenosine receptor as a physiological immunosuppressor and to engineer inflammation in vivo. *Biochem Pharmacol*. 2003;65(4):493-501.
 64. Sitkovsky MV, Lukashov D, Apasov S, et al. Physiological control of immune response and inflammatory tissue damage by hypoxia-inducible factors and adenosine A2A receptors. *Annu Rev Immunol*. 2004;22:657-682.
 65. Ralevic V, Burnstock G. Receptors for purines and pyrimidines. *Pharmacol Rev*. 1998;50(3):413-492.
 66. Song N, Li T. Regulation of NLRP3 inflammasome by phosphorylation. *Front Immunol*. 2018;9:2305.

SUPPORTING INFORMATION

Additional supporting information may be found in the online version of the article at the publisher's website.

How to cite this article: Mezzasoma L, Bellezza I, Orvietani P, et al. Amniotic fluid stem cell-derived extracellular vesicles are independent metabolic units capable of modulating inflammasome activation in THP-1 cells. *FASEB J*. 2022;36:e22218. doi:[10.1096/fj.202101657R](https://doi.org/10.1096/fj.202101657R)